JOURNAL OF MATERIALS SCIENCE **34** (1999) 2955–2969

Mechanical and tribological properties of Hadfield steel coatings manufactured by laser processing

J. M. PELLETIER
GEMPPM-Calfetmat, INSA, Bat. 403, 69621 Villeurbanne Cedex, France
E-mail: pelletie@insa.insa-lyon.fr

E. SAUGER, Y. GACHON, A. B. VANNES
IFOS-Calfetmat, ECL, Avenue Guy de Collongues, 69131 Ecully Cedex, France

For a lot of applications in the mechanical industry, materials combining both attractive mechanical properties and enhanced wear resistance are required. Usually such a combination is achieved only by performing surface treatments, especially by manufacturing coatings with the appropriate composition and microstructure. Laser cladding is an innovative and attractive manufacturing route. Ceramic or metal-matrix composites are possible candidates in some circumstances. However their low plastic deformation ability limits their use. The present works reports on metallic coatings (Fe-Mn-C steels, known as Hadfield steels). They are obtained by laser cladding (direct injection of powder into the laser beam) and then characterised by metallurgical, tribological and mechanical analysis. Directly after manufacturing, Hadfield steel coatings are sound, metallurgically bonded to the substrate and with an austenitic structure. Their mechanical features are fairly good: hardness HV = 350, Young modulus: $E = 210$ GPa, yield strength: $\sigma_E = 1200$ MPa. However, the most attractive features are as follows:

—they are very ductile: relative deformations higher than 80% are achieved without intermediate annealing and without deleterious damages. This deformation yields to a large work-hardening phenomenon, since hardness values higher than 800 HV are measured.
—wear observed during fretting tests is limited and delayed, whatever the nature of the regime: elastic or plastic.

A metallurgical analysis indicates that this behaviour is due to a twinning phenomenon, at least in a particular deformation range.

1. Introduction

Development of advanced materials combining both interesting intrinsic mechanical properties and high wear resistance in diversified conditions of use is the subject of a lot of work, since scientific, technological and economic problems are involved. Significant improvements have been achieved by performing surface treatments, since suitable composition and microstructure can be obtained. Processing with high energy beams makes it possible to get very fine microstructures, induced by the inherent rapid solidification, with a high potential for developing wear resistant layers. Laser cladding is a promising technique [1].

Among the advanced materials with good tribological properties, metal matrix composites have received considerable interest in the past years. Reinforcing particles (carbides, oxides, . . .) are dispersed in a ductile matrix (typically an aluminium- or a nickel-base matrix). Processing with laser yields an enhanced abrasive wear resistance. For instance, weight loss after a classical pin on disk test are significantly reduced, compared to a more conventional material [2–10].

However, this class of alloys is faced with two kinds of problems [11–13]:

- plastic deformations which can be performed without damage is very limited (usually less than 10%). This poor room temperature ductility hinders processing of metal matrix composites, either bulk materials or surface coatings.
- the composite nature of these materials leads to residual microstresses, owing to differences in coefficient of thermal expansion (CTE) between reinforcing particles (or fibres) and matrix. Therefore, macrostress damage accumulates and cracking can be observed during the life of the workpiece submitted to complex loading (especially when tensile stresses are induced).

These drawbacks are much smaller in homogeneous metallic alloys. Unfortunately, their mechanical

properties (hardness, Young modulus, . . .) are poor. Manganese steels known as the Hadfield steels (with a manganese content of about 12% and a carbon content of about 1.2%) is a specific case, since a large work-hardening phenomenon is observed during a plastic deformation. Bayraktar *et al.* [14, 15] have, for example, performed tensile tests with these steels and they reported that strengthening is very important, even when tests are carried out at fairly high temperature (up to about 400 °C). Toughness is very large and, consequently a high wear resistance is expected.

The present work reports on works performed in CALFETMAT (INSA and Ecole Centrale de Lyon) in this field. First, the manufacturing route will be described; then the resulting microstructure and static mechanical properties (initial hardness and influence of cold working rate on hardness) will be presented. Finally, the paper will conclude with dynamic tests: fretting tests, erosion wear tests, in connection with microstructural observations.

2. Experimental procedure

A CW CO2 laser, CILAS CI4000, with a maximum power of 4 kW, was used. Laser beam was focused on the workpiece using a 10 inch ZnSe lens. Working distance was adjusted in order to produce a spot with a diameter of 3 mm on the sample surface. The specimen ($100 * 50 * 10$ mm^3) was an annealed low carbon steel (0.2%C). The powder had the following composition Fe-12% Mn-1.2% C and the granulometry was in the range 40–100 μm. It was injected through a coaxial nozzle, with argon gas acting as support. The powder feed rate was adjusted using a powder injection system (Plasma Technik TWIN 10C).

Specimens were mounted on a numerically controlled X-Y table. Scanning speed under the laser beam was in the range 5–20 mm/s. Parallel tracks, with a shift δ (about 50%), were carried out, in order to generate large surfaces.

The microstructure was observed on a cross-section, after polishing and etching with nital. EDS (electron dispersive spectroscopy) was also performed to get information on chemical analysis. X-ray diffraction experiments, with CuK_α radiation, revealed the various phases. Finally, hardness profiles were achieved on cross-sections.

3. Manufacturing and characterisation of coatings

Hadfield steel claddings were manufactured using processing parameters retained for similar metallic claddings, like Co- or Ni-base alloys, with similar thermo-physical features [16]. However, a selection of suitable processing conditions was required to obtain good claddings, i.e. sound layers (without pores or cracks), homogeneous layers (without undissolved particles) and good bonding between cladding and substrate.

The microstructure, resulting from the processing itself, is very fine. Fig. 1 shows that the cladding is homogeneous, dense and sound, with a dendritic microstructure and a metallurgical bonding to the substrate. This homogeneity results mainly from the fact that preallied powders have been used. Indeed, as shown in previous papers [17, 18], it can be very difficult to get a homogeneous coating using simultaneous projection of different powders presenting very different features: for example, mixing Al, Cu and Fe powders to manufacture an homogeneous Al-Cu-Fe coating is very difficult, since, on the one hand, laser-material interaction phenomena are very different for the various elements (specific reflectivity) and, on the other hand, thermophysical properties are dissimilar (melting temperature, thermal conductivity, . . .).

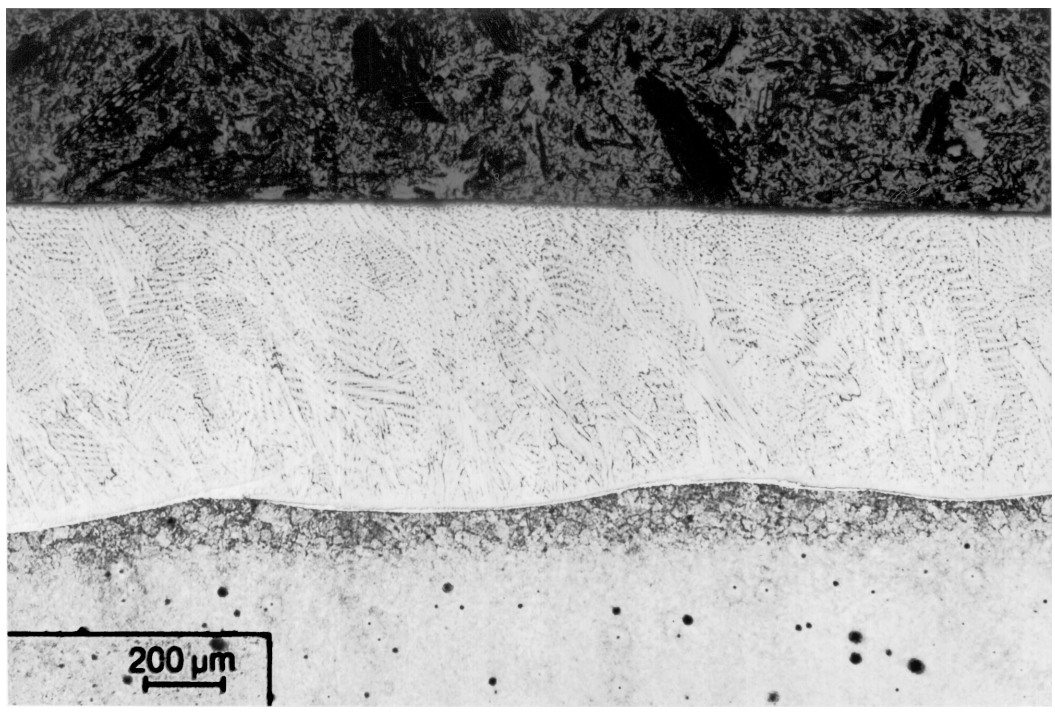

Figure 1 Micrograph of a typical coating.

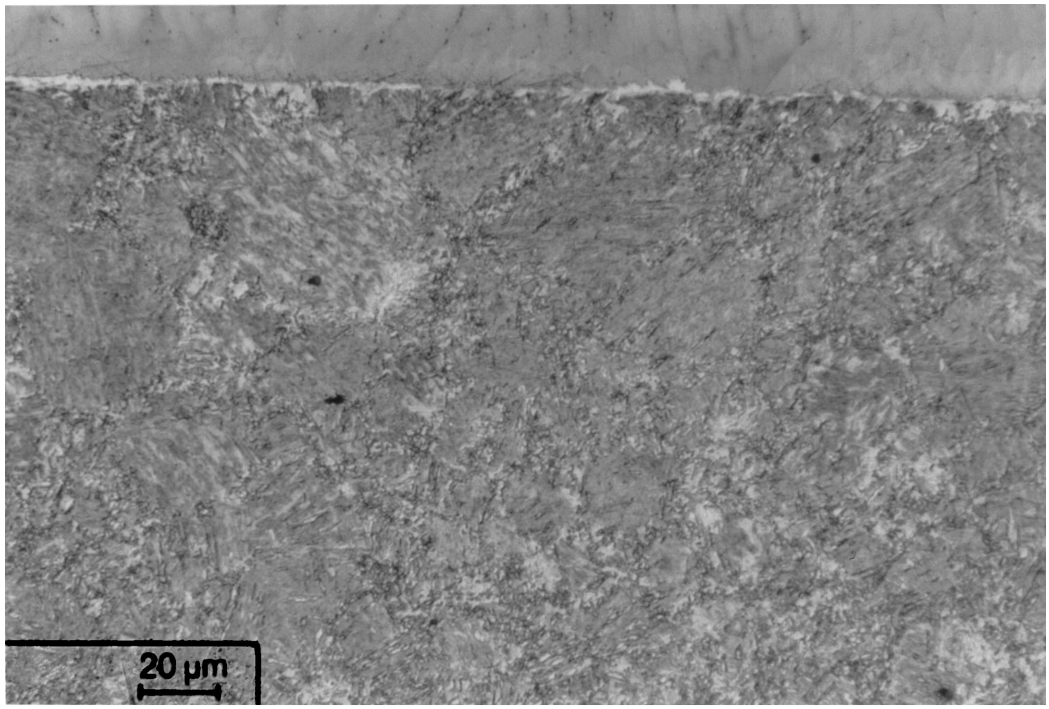

Figure 2 Microstructure of the HAZ.

Homogenisation would require an increase of the melt pool lifetime to enhance interdiffusion of the elements (especially by convection). Unfortunately, coating quality is then reduced: *a too important melting yields* inevitably to an excessive dilution of the substrate and, consequently, to a worsening of the coating composition compared to the initial powder composition.

The microstructure of the substrate is classical for an annealed carbon steel. In contrast, the microstructure of the heat affected zone (HAZ) is more complex (Fig. 2): the shorter the distance to the coating-substrate interface, the higher the temperature during the processing, yielding to a higher dissolution of perlite during heating and to a larger formation of martensite during cooling. Therefore, progressive evolution of the microstructure is observed: when moving from the interface the microstructure goes progressively from a martensitic structure to a cellular structure containing perlite and ferrite.

X-ray diffraction patterns show that Hadfield coatings (like bulk Hadfield steels) are constituted by an austenitic phase, with a face centred cubic structure, similar to that of austenitic stainless steels (ASTM 31-619). The lattice parameter of the cubic phase, calculated from the location of the most intense peak (111) is slightly higher ($a = 0.362$ nm) than that of the ASTM file ($a = 0.360$ nm); the difference is simply due to the distortion effect introduced by carbon and manganese atoms in solid solution in iron (both elements favours the formation of the γ-iron phase).

EDS microanalysis, performed using a scanning electron microscope, indicates that manganese content in the coating (10.8%) is very close to the initial powder one (about 12%). Therefore, dilution is limited and, anyway, this content is in the suitable range for Hadfield steels.

The average microhardness of these coatings is about 350 HV. Young modulus E and yield strength $\sigma_{0.2}$ have been determined using an hertzian indentation technique [19]: $E = 210$ GPa, $\sigma_{0.2} = 1200$ MPa.

4. Plastic deformation of coatings

In order to investigate workhardening in Hadfield steels, two parallelepiped samples have been prepared: one was cut off so that it contained the sample proportion of coating and substrate, the other one contained only the Hadfield coating. Cold working was progressively performed with an increasing ratio in a direction parallel to the laser scanning direction. Workhardening was quantified using microhardness measurements and evolution of the crystalline structure was investigated by X-ray diffraction experiments and optical micrography.

4.1. Hardening curves

The *sample containing both substrate and coating was progressively plastically deformed* up to a ratio of 80.5%. After a given deformation ratio, hardness measurements were carried out both on substrate and Hadfield cladding, in order to compare the effect of a plastic deformation. Results are given in Fig. 3a.

Hardening in the substrate was low. Indeed the hardness increased only from about 200 in the undeformed material to only about 280 after a very large deformation (about $70 < \%$).

Directly after manufacturing, the cladding is still harder (350 HV), but the main result is the important linear increase of the hardness resulting from the coldworking: indeed hardness values up to 800 HV are achieved after a deformation ratio of about 80%. Let us mention the ductile behaviour of this cladding, since very large plastic deformation can be obtained without deleterious cracking.

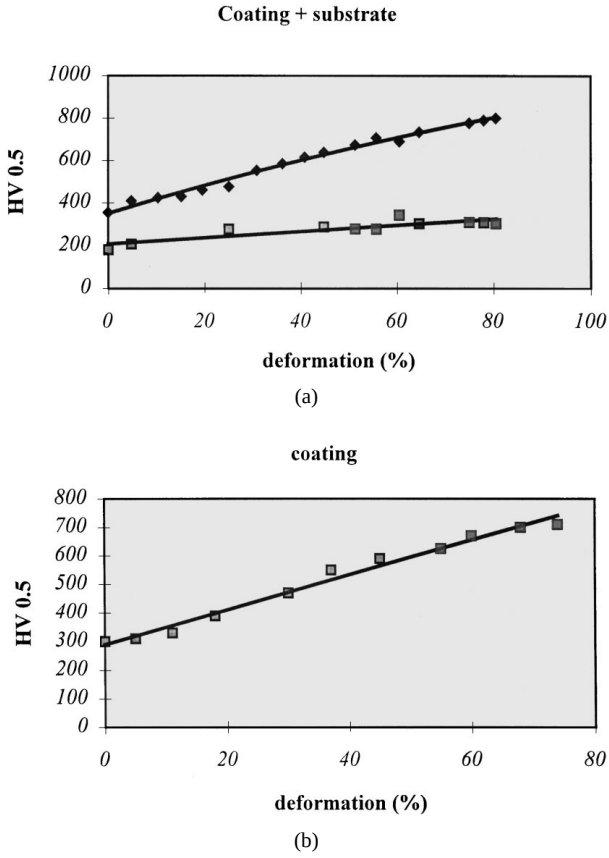

Figure 3 Hardness versus deformation ratio: (a) coating + substrate; (b) substrate alone.

The specimen bends during the test when the deformation ratio exceeds about 20%; indicating therefore a difference in the behaviour of the two materials (substrate and coating) during cold working. Since workhardening in the substrate is more limited, its deformation tends to be higher, yielding to internal stresses in the specimen and consequently to the observed bending.

No scaling phenomenon is observed on the surface of the specimen (no 'orange peel formation'). Only small cracks can be detected on the edges, when the deformation ratio exceeds about 50%.

The specimen containing only the Hadfield cladding was coldworked in a similar way. The same behaviour was observed: a linear hardness increase up to about 750 HV for a deformation ratio of about 75% (Fig. 3b). No orange peel formation was detected.

4.2. The microstructure of the deformed samples

The specimen containing both cladding and substrate was cut after various cold rolling ratios, in two directions parallel or perpendicular to the laser track), polished and etched in nital, in order to investigate microstructure evolution during plastic deformation.

A longitudinal cross-section of the sample is shown in Fig. 4 (the deformation ratio here is 80.5%). Texture and elongation of the microstructure in the cold-working direction are clearly observed. Grains are elongated, both in substrate and cladding. Only a few cracks are visible. In contrast, a lot of small dark spots are located along the grain boundaries; they seem to follow the movement of the deformed matter. They may be either pores or defects resulting from preferential etching by nital in grain boundaries. In spite of the very high cold-deformation ratio no debonding appears at the substrate-cladding interface. Metallurgical bonding is, therefore, very strong and prevents any scaling phenomenon.

Cracks which cross the sample originate from cracking on the edges of the specimen and then propagates throughout the cladding.

Even when a detailed observation is performed, with a high magnification (up to 1000), no martensite and no twins can be detected in the cold-worked coatings. However, this plastic deformation technique, which allows a very large deformation ratio, is perhaps not the most suitable technique to properly observe defects induced by the deformation. We will discuss this point later on.

Scanning microscope observations confirm these results: the microstructure is dendritic after manufacturing, remains dendritic after the plastic deformation and a texturing effect appears and substrate and coating remain metallurgically bonded, even after a drastic deformation. Nevertheless, some cracks can be observed at the interface, when a very high magnification (>1000) is used. On a longitudinal cross-section (Fig. 5), some areas show some kinds of parallel lines, with only a slight contrast, in the sample constituted by substrate and coating, after a very high deformation. This 'stretching' phenomenon could result from a twinning process. However, further investigation is required. A particle embedded in the substrate is also visible on this micrograph.

5. Fretting behaviour of Hadfield steel claddings

5.1. Introduction

Many industrial structures show limited lifetimes either because of injuries in quasi-static equipment or as a result of damage created in parts which are put together in contact. Small displacements appear between the contact surfaces under cyclic loading conditions. These small displacements result in a loss of matter [20] or in crack initiation [21]. Such kind of damage is called "fretting."

The test used in this study was designed and developed at Ecole Centrale in Lyon, in the MMP-IFoS Department [22]. Its consists of a special tribometer which applies an alternative motion of low amplitude to two samples (called "first bodies"). One of the samples is fixed on a rigid frame whereas the other is connected to the piston of a tensile-compressive servo-hydraulic equipment moving at imposed displacement D (low amplitude: typically a few dozens of microns) and chosen frequency ($f = 1$ Hz from the standards). F_n is the normal load and is continuously recorded during the tests and applied via a loading rectangle. Moreover, one of the samples is shaped as a sphere or a cylinder which allows accurate calculation of the imposed stress and strain fields. Tests are run at room temperature (23 °C) and a humidity level of 40% R.H.

The tangential load F_t is continuously recorded as a function of the relative displacement D. This recording

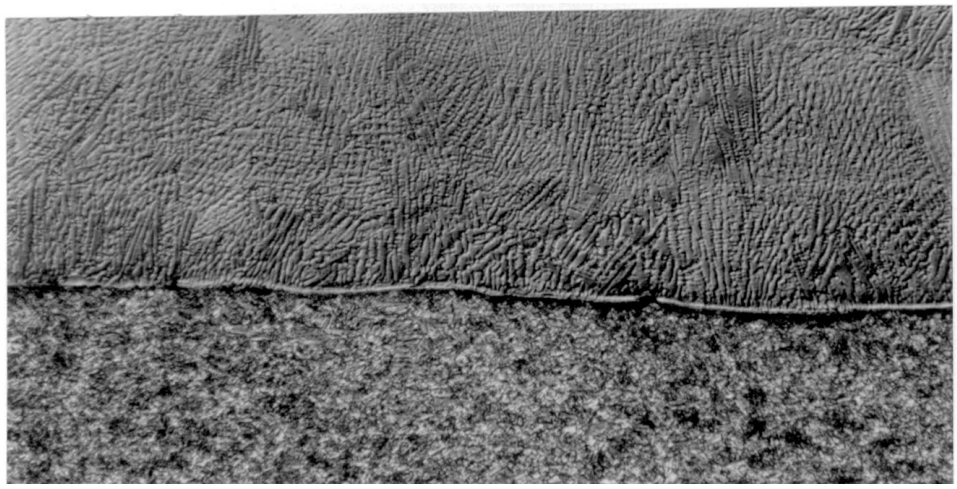

(a)

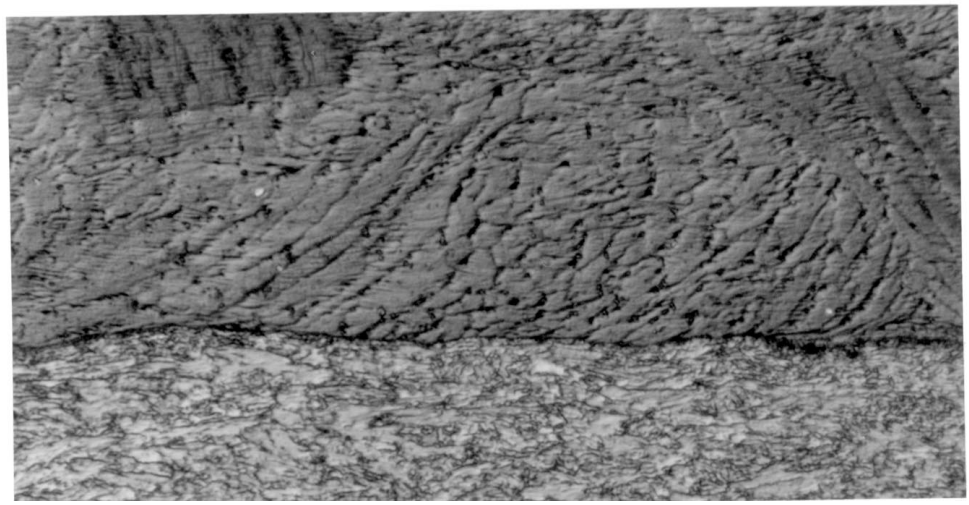

(b)

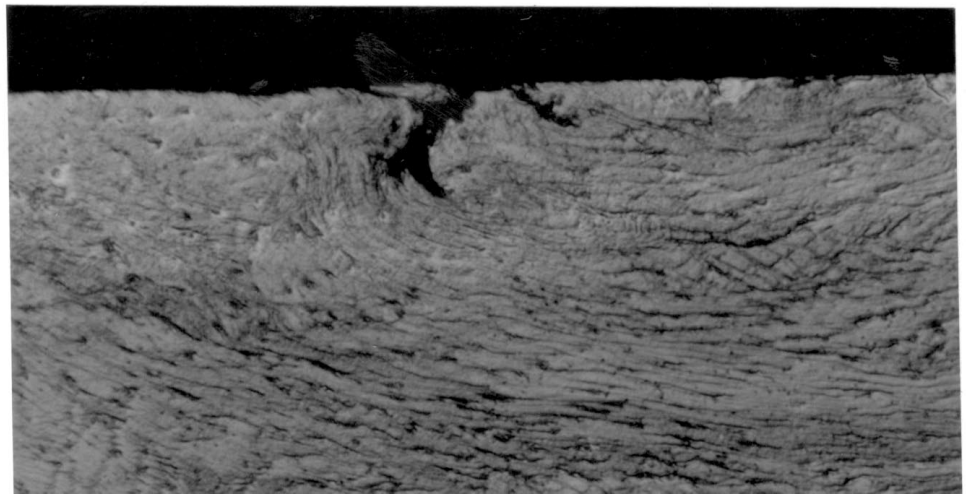

(c)

Figure 4 Longitudinal cross-section of the sample with coating and substrate. (a) $G = x20$. Overall view. (b) $G = x500$. Movement of the textured material. No debonding at the interface. (c) $G = x500$. Crack through the specimen.

leads to the plot of F_t-D fretting curves all throughout the test. When these F_t-D curves are superimposed to a third axis, which is a function of the number of cycles, we end up with the so-called three-dimensional "fretting logs" [22].

Three kinds of F_t-D curves are currently encountered during fretting tests:

(i) closed curves, which look like a very flat ellipse: the tangential load increases linearly with the

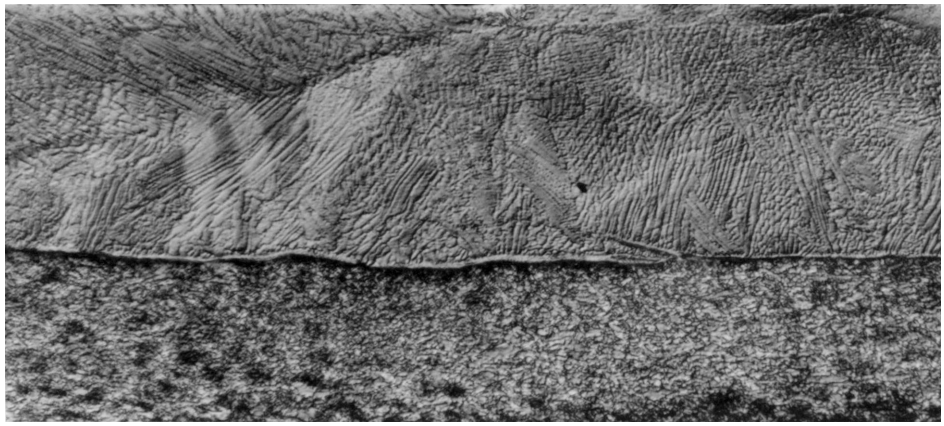

Figure 5 Longitudinal cross-section of the sample with coating and substrate, after cold rolling (80%), $G = x1000$.

displacement, and the relative motion of the two samples remains negligible. The elastic strain of the system test rig + sample is high enough to take the relative displacement into account. The materials tested are hence subjected to conventional tensile-compressive fatigue.

(ii) elliptic curves: F_t increases in a non-linear way with the displacement. In this case, an annular-shaped area (in the case of a sphere-on-flat contact) slips and is located at the border of the contact. The centre of the contact remains nevertheless stuck, and the contact is hence subjected to partial slip. Thus the materials are tested in oligo-cyclic fatigue.

(iii) parallelogram-shaped curves: at first, F_t increases linearly with D as in case (i), but then, beyond a threshold value, reaches a plateau or increases at a much slower rate. This kind of F_t-D curve is a characteristic of gross slip. The friction coefficient μ is then equal to F_t/F_n. Damage in the materials is characterised by wear and is more or less controlled by the creation of a "third body" made of debris.

In some cases, the mechanical response of the contact may change and mix several cases among the three mentioned above. We thence speak of "mixed regime" [21]. Moreover, two situations must be considered during static loading. The initial contact pressures may either be lower than the yield stress, as calculated by the Hertzian theory; or be higher and lead to local plastification. This latter case is considered as the severe loading conditions.

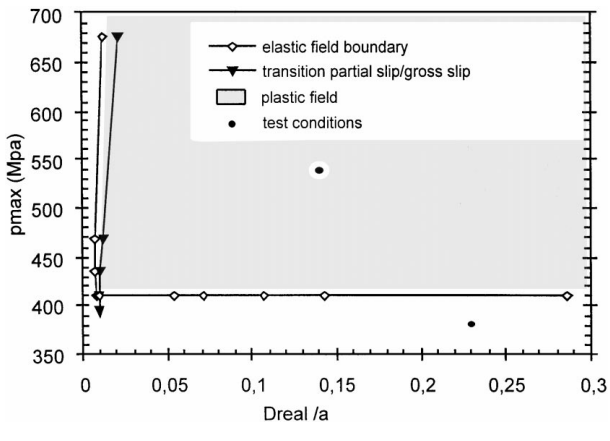

Figure 6 Elastic and plastic fields for fretting tests (from [23]).

From data on the materials and calculations derived from the Hertzian theory [23], we may plot a curve such as in Fig. 6 where the various loading fields are shown. From our study in gross slip conditions, we considered the two cases for the initial contact pressures quoted previously. Furthermore, for elastic loading conditions, the tests were calibrated to avoid overstress resulting from the relative displacement of the two contact surfaces. We ensured that this overstress remained lower than the σ_y of the sample tested.

All tests were characterised by three factors: their tribological behaviour, their change in micro-hardness and their metallurgical observation.

5.2. Gross slip tests under severe loading conditions in the plastic field

In this part of the study, we chose a sphere-in-flat contact geometry. The sphere was made of 100C6 ($\sigma_y =$ 1700 MPa) and the flat surface was made of one of the following materials:

—Hadfield coating.

—35NCD16: this is a low alloyed steel with a martensitic metallurgical structure. This steel was quenched in oil but not tempered which account for its brittle behaviour ($\sigma_y = 1600$ MPa).

—Z0.03CN18-10: this is an austenitic stainless steel with a ductile behaviour ($\sigma_y = 440$ MPa). The 100C6 sphere had a higher curvature ($R = 50$ mm instead of 11.5 mm). This ensured that the ratio σ_y/P_{max} remained constant for all materials, where P_{max} is the maximum Hertzian pressure in the contact.

5.2.1. Analysis of the results

The change in the friction coefficient of the Hadfield coating may be divided into three stages:

A. At first, μ increases with the very first cycles until reaching $\mu = 1$ after 200 cycles.

B. μ falls afterwards and reaches a plateau around 0.7 located between 20 and 2000 cycles.

C. Eventually, μ shows a secondary peak around $3 \cdot 10^4$ cycles and then decreases with the number of cycles until the test is stopped (after 2.5×10^5 cycles).

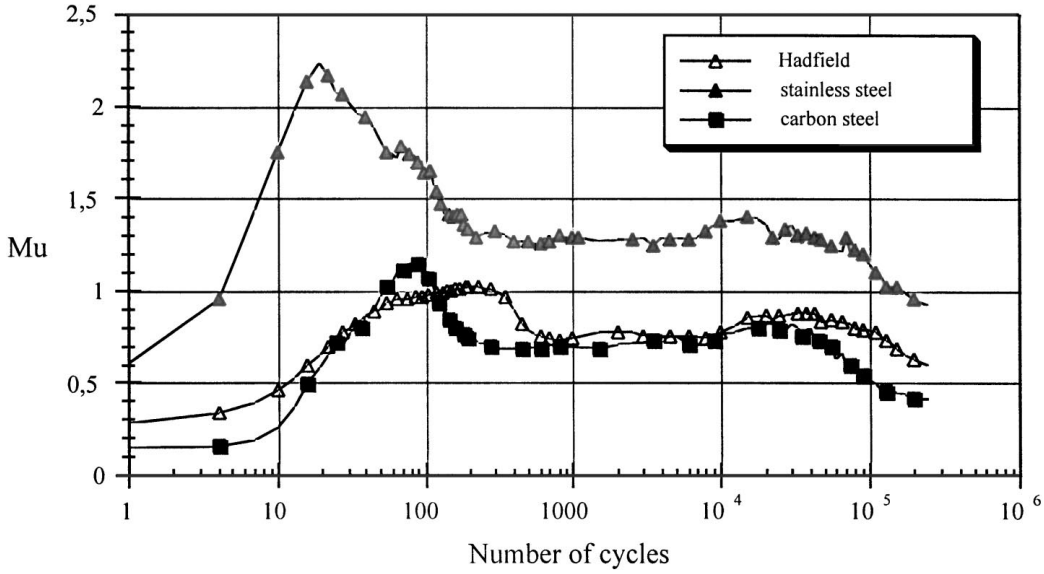

Figure 7 Evolution of the friction coefficient as a function of the number of cycles.

The other materials tested had pretty similar changes in their friction coefficients. In fact, the part A is a running-in period. The fine layers of oxides or pollutants, which lie on the surface of the sample as "first bodies" are destroyed and expelled from the contact. Local microwelds are created with early plastic strains and result in an increase in the friction coefficient during the first hundred cycles. But small differences still remain among the various materials tested (Fig. 7):

(i) The friction coefficient for the stainless steel increases steeply with the very first twenty cycles up to $\mu = 2.2$ (growth rate $\tau = 95 \cdot 10^{-3}$ cycles^{-1}).

(ii) The friction coefficient for the 35NCD16 steel follows the same trend and ends up around $\mu = 1.2$ after 80 cycles (growth rate $\tau = 10^{-2}$ cycles^{-1}).

(iii) But evolution of friction coefficient for the Hadfield steel versus number of cycles follows two steps: up to 40 cycles, μ has a steeper increase than in the case of the low alloyed steel (growth rate $\tau = 2 \cdot 10^{-2}$ cycles^{-1}) and then reaches its maximum value around 200 cycles but at a slower rate ($\tau < 10^{-3}$ cycles^{-1}). This slower part could be explained by strain hardening phenomena which lessen the material's strain ability. Hadfield coating is therefore more ductile than low alloyed steel ($\tau > 10^{-2}$ cycles^{-1}), and ends up in a more brittle one ($\tau < 10^{-2}$ cycles^{-1}).

The fall in friction coefficient which occurs around 200 cycles (however much earlier for stainless steel) is a result of debris creation. These first debris take account of part of the relative displacements, and lower applied stress on first bodies [20]. This is a positive issue of particle detachment. The duration of this phenomenon is however independent from the material tested and takes about 200 cycles long before μ reaches a plateau. At that time, and unlike the steep increase in μ described previously, the material's nature would no longer monitor debris growth but still affects it by the shapes of the curves. The test frequency seems nonetheless to become the main parameter but there is a need for further investigation of this assumption.

We would like to point out that these first debris might as well come from material's tested surface or from the antagonist (sphere). Analysis performed in EDS on fretted surfaces, however, showed no important amount of matter coming from the fretting sphere. In the next step, the debris particles change their size, were oxidised and ultimately totally expelled from contact. From this last step on, the name of "wear" may properly be used. Debris action (or third body action) is now lowered, and a new period of adaptation comes into action resulting in a small increase in μ around 10^5 cycles. Let us also note that normal load decreases at that time, since the testing rig was not designed to stop the relative inner displacements in contact due to matter loss. We hence get information on wear kinetics under constant normal pressure (Fig. 8). These plots can therefore not be considered quantitatively but for relative comparison.

In Fig. 8, we notice a fall in F_n/F_{n_o} (where F_{n_o} is the initial normal load). Still, this fall is less important and occurs later for both the Hadfield and stainless steels. We remind the reader that a larger sphere was used when testing this latter material (cf. Section 5.2). This geometry resulted in a broader wear track (4 mm in diameter instead of 2 mm). It is thence easy to understand that debris trapping is more efficient in the case of a broader track and with more adhesive particles. However, the wear is smaller and belated for Hadfield steel. This phenomenon may be a consequence of the strain hardening process.

5.2.2. Analysis of wear tracks

Pictures 1 and 2 of Fig. 9 were taken in polarised light and show the global view as well as detail of a fretting track on the Hadfield steel after 5000 cycles in gross slip ($F_n = 300$ N and $D = \pm 30$ μm). On this track, there is a strongly damaged area with debris almost all over its surface. In the centre of the track, a less damaged area appears lighter and full of fretting scars. The width of these scars decreased with the number of cycles and eventually disappeared. In addition to the fretting track, some "terrace-shaped surface" may be seen ahead of the contact area as well as behind it. These "terraces"

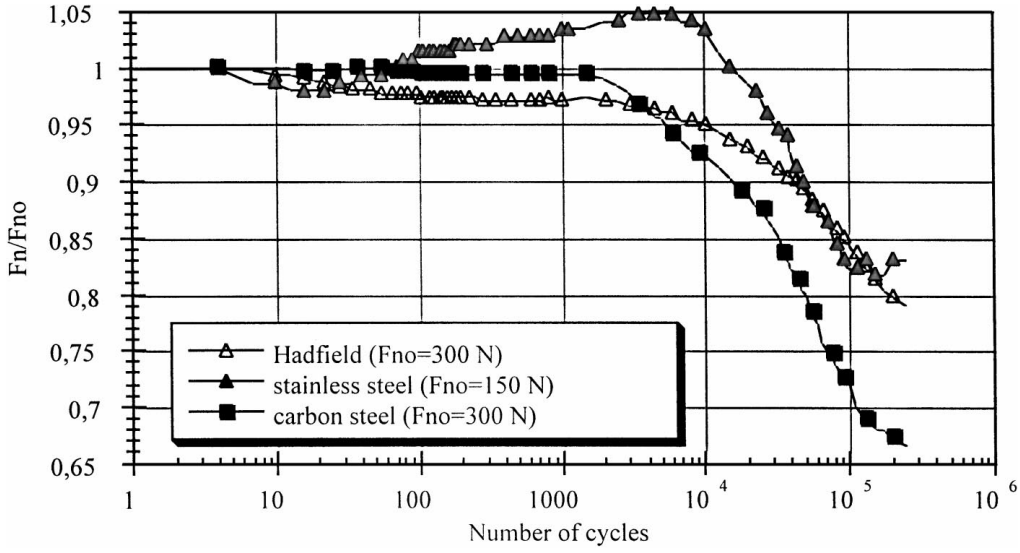

Figure 8 Evolution of the normal load as a function of the number of cycles.

are probably linked with twin formation which is a characteristic of this steel. Their location is the result of high tensile and compressive stress generating high plastic strains in this area.

In the case of stainless steel, its wear tracks looked much alike. Still, we were concerned with sliding stripes instead of twins.

5.3. Gross slip tests in the elastic field

We used a cylinder-on-flat geometry to ensure elastic strains and to broaden the contact size (contact radius $R = 50$ mm, contact width $l = 8$ mm). The maximum Hertzian pressure was thence lowered to the threshold for which plastic deformation was not encountered [23]. Here again, the antagonist was made of 100C6.

5.3.1. Analysis of fretting logs

From the observation of Fig. 10 (friction coefficient μ), we can easily derive three stages:

1. μ increases up to 0.8 during 20 cycles
2. μ shortly decreases during 80 cycles
3. μ increases again, but at a much slower rate and reaches its maximum value ($\mu = 0.9$) around $3 \cdot 10^4$ cycles. Then μ eventually decreases until the end of test.

We shall now try and explain these changes in friction coefficient by comparing them to what has happened in the plastic zone field.

First the increase is linked to adaptation as shown previously. After 20 cycles, the very first debris appear and lead to a drop in tangential load F_t and so far in μ. The initial stress field is no longer high enough to create plastic strains which would change the interactions between first bodies. So the maximum peak in μ at 200 cycles is not observed. However, light surface damage occurs and generates more severe injuries to the material, even though smaller loads were applied. This leads to a progressive increase in μ which in turn affects local plastic strains and strain hardening associated phenomenon. Debris particles then appear and are turned into oxides or smashed debris which are expelled from contact.

In this case, we are dealing with a more progressive and more continuous process. The tribological states determined after $3 \cdot 10^5$ cycles in the two latter cases are however pretty similar: the history of the first bodies is gradually forgotten and contact behaviour is governed by third body mechanical behaviour.

5.3.2. Study of F_n/F_{n_o}

In Fig. 11 we easily see that the normal load falls from 5% between 10 and 30 cycles in the presence of an elastic stress field. This fall is the result of local running-in and first debris nucleation. It is all the more important since the strain hardening phenomenon has not started to this point. Indeed, we see that the more severe the stress field, the lower the fall in F_n.

During the next stage, changes in stress field and in normal load look similar. This confirms the analysis made on both the friction coefficient and third body as an essential part in the wear process. In fact, after a plateau region, F_n/F_{n_o} decreases quickly around 10^5 cycles because debris are expelled from contact. The oscillatory frequency remains the key-parameter in this ultimate part of test. Moreover, the elastic stress field shows a drastic fall beyond $6 \cdot 10^4$ cycles. This acceleration is for sure a result of a poorer ability to particle grasping of the cylinder-on-flat geometry. But it could also be a consequence of a slower supply of third body resulting from a larger strain hardening phenomenon.

5.3.3. Observation of wear tracks

At a lower number of cycles, we found again a "terrace-shaped" surface at the border of the contact. We also found a layer of oxidised debris gradually covering the fretting track area.

At 2.5×10^5 cycles, the track area looked very torn out with a large amount of debris located at the border of the contact (Fig. 12). Micro-hardness measurements (Fig. 13) were performed after the fretting tests.

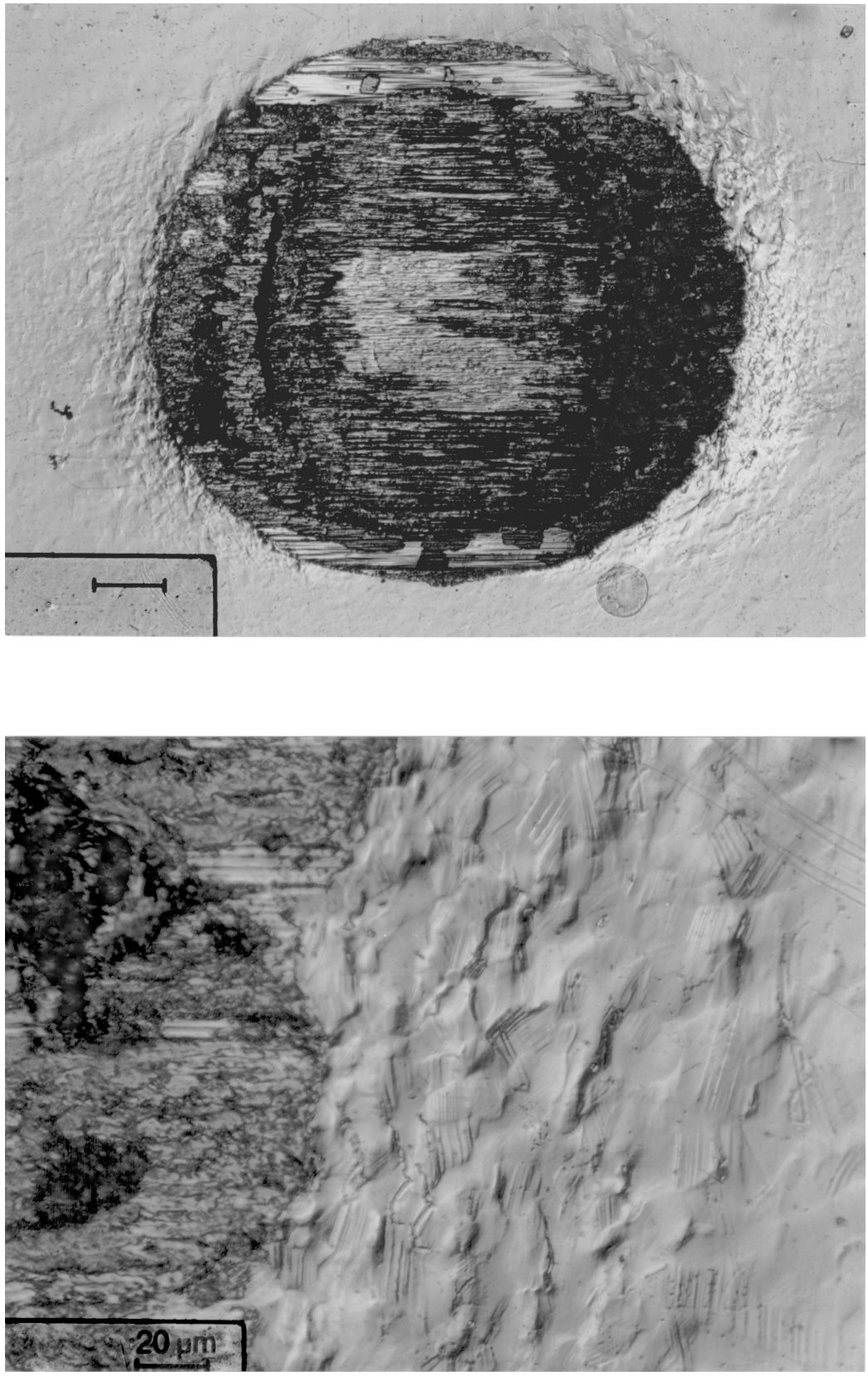

Figure 9 Micrographs of wear scars.

They followed the friction direction and started from the centre of the track. Results show a higher hardness inside the contact than found at its border. Still, these results are pretty similar to the ones taken on tracks tested under severe plastic loading conditions. The latter, however, gave evidence of harder small "islands" of 1000 to 2000 $HV_{0.025}$ located close to the centre. But the strain hardening phenomena were more developed in the plastic field, so that these residual harder areas are not surprising. Furthermore they seem to resist wear more. Once again, this observation emphasises the previous conclusions on changes in the friction coefficient and in F_n/F_{n_o}.

A longitudinal cross-section of the sample gives evidence for twins and superficial cracks which may lead to chipping (Fig. 14). Micro-hardness measurements

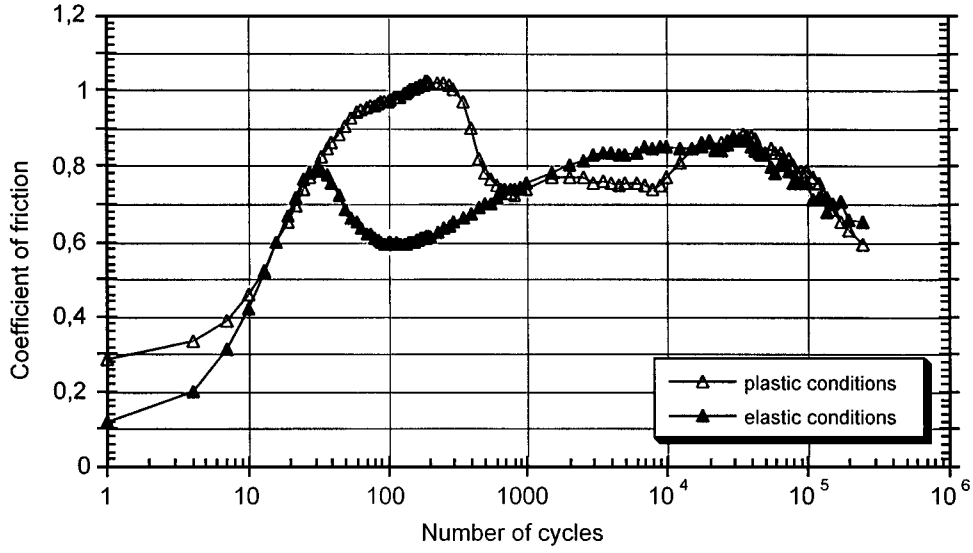

Figure 10 Evolution of the friction coefficient as a function of the number of cycles.

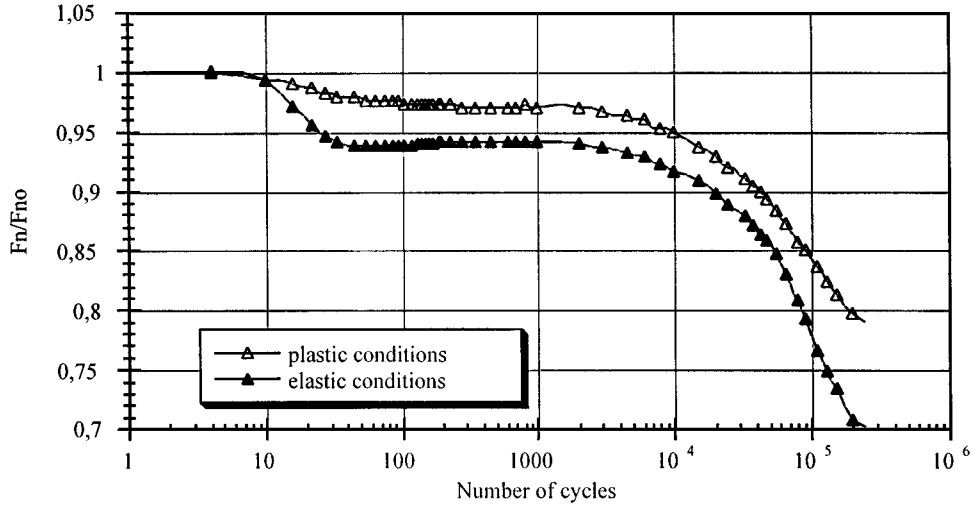

Figure 11 Evolution of the normal load as a function of the number of cycles.

in that area showed important hardening due to the strain hardening phenomena (570 $HV_{0.015}$ in that area whereas only 320 $HV_{0.015}$ in depth).

6. Erosion resistance of Hadfield steel claddings

The impact of particles on a surface can cause severe erosion damages. Erosion of a surface by abrasive particles (sand for example) in an inert fluid depends on a lot of parameters: the number of particles, their mass, their geometry, their size and direction relative to the surface. This type of wear affects many industrial sectors: aeronautics, hydraulic and pneumatic industries, and so on. For the present study, a specific bench test was used [24, 25]. The erosion rate is simply defined by the ratio of the weight loss of the sample and the mass of the impinging particles. In ordre to estimate the erosion resistance of Hadfield steel coatings, comparative tests have been performed on various materials: a titanium alloy (Ti-6% Al-4% V), a stainless steel (316L), a nickel base superalloy (Ni-22% Cr-Fe-Mo) and a plasma sprayed carbide coating.

6.1. Results on Hadfield coatings

Table I lists the conditions of test. A mass of 1 g make it possible to observe the elementary mechanisms of erosion wear, while a larger mass corresponds to a more realistic test of erosion resistance. A curve relating the influence of the impact angle on the erosion rate was achieved using a projected mass of 200 g.

Processing conditions are as follows:

- average diameter of sand particles: 250 μm
- Distance between nozzle and specimen: 30 mm
- Average particle velocity: 100 m/s

Results are plotted in Figs 15 and 16. The curve relating the erosion rate as a function of impact angle (Fig. 15) was decomposed into two components, according to the analysis of Neilson [26]. The maximum magnitude of these two components are similar. Therefore it can be concluded that the tested material exhibits a behaviour which is intermediate between that of a brittle material and that of a ductile material.

Fig. 16 shows that the eroded depth increases linearly with the projected mass. Eroded depth was measured in the centre of the eroded zone.

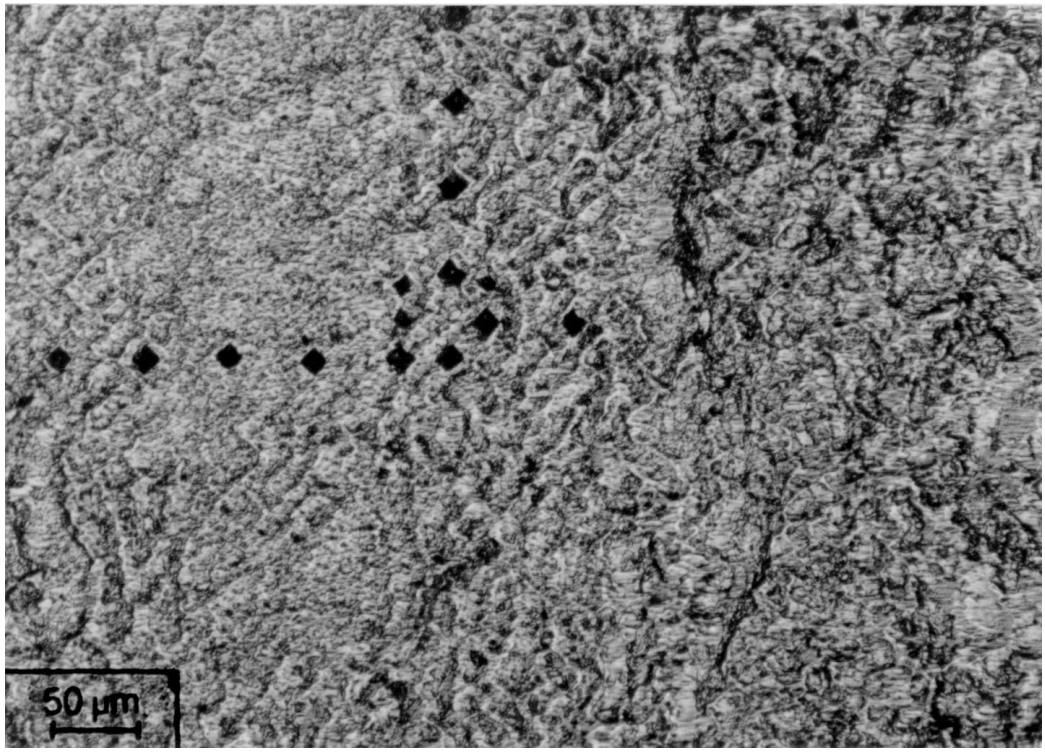

Figure 12 Micrograph of a zone after 250,000 cycles of fretting.

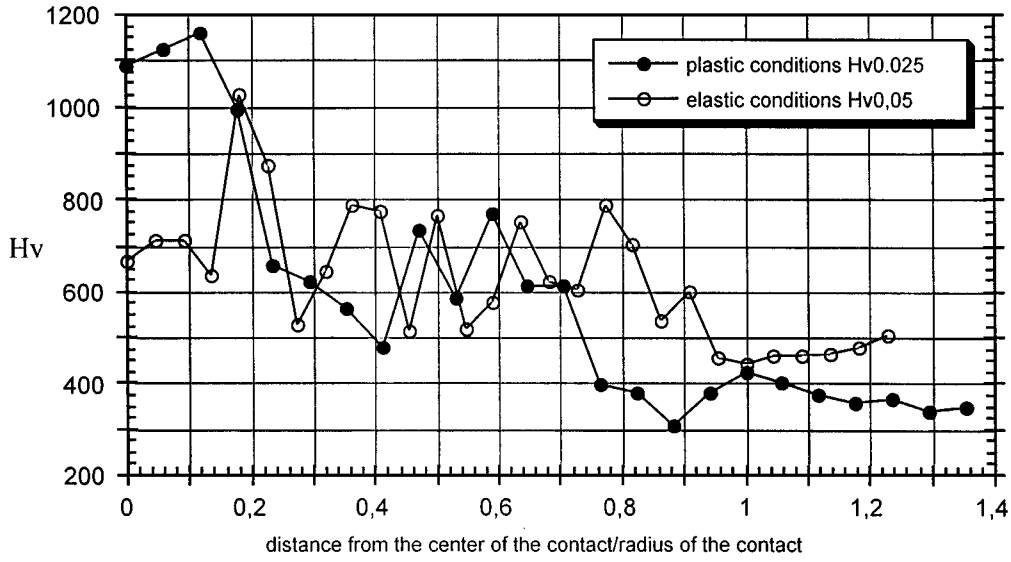

Figure 13 Hardness profile on a cross-section.

6.2. Comparison between Hadfield steel and other materials

Fig. 17 reports the erosion rate of various materials as a function of the impact angle. In order to compare in a significant way the results achieved in materials with very different density, erosion rate is measured as volume loss. Whatever the impact angle, the Hadfield steel shows a better erosion resistance than the other materials (excepted the austenitic stainless steel for $\alpha = 90^{\circ}$). Note that erosion rate relative to the Hadfield steel coating depends only slightly on the impact angle in the range 30–90°, in contrast to what is observed in other materials in metallic alloys, the erosion rate decreases with a, while in brittle materials an increase is observed. In order to determine the physical origin of this good erosion resistance, cross-section of these specimens were carried out in the middle of the erosion scar and a hardness profile was then performed (Fig. 18).

Measurements have been achieved below a digging scar produced by the impact of a single particles (or only a few ones). A large hardening is observed in a thin layer, the thickness of which is about 20 μm for a very low projected mass, 1 g. Consequently, hardening takes place since the first particle impacts. Shimizu and Noguchi [27] have reported a similar observation in austenitic cast irons.

Another cross-section performed throughout a scar induced by a projected mass of 50 g indicates that the thickness of the hardened layer is then 60 μm. In such

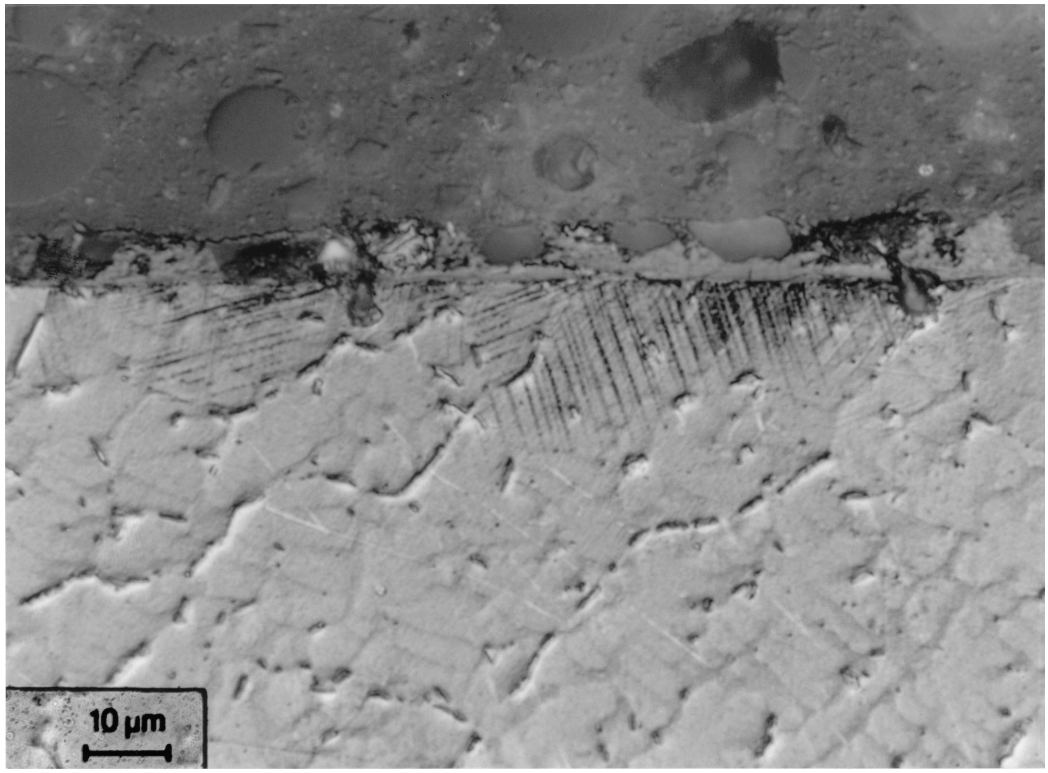

Figure 14 Longitudinal cross-section on a fretting scar.

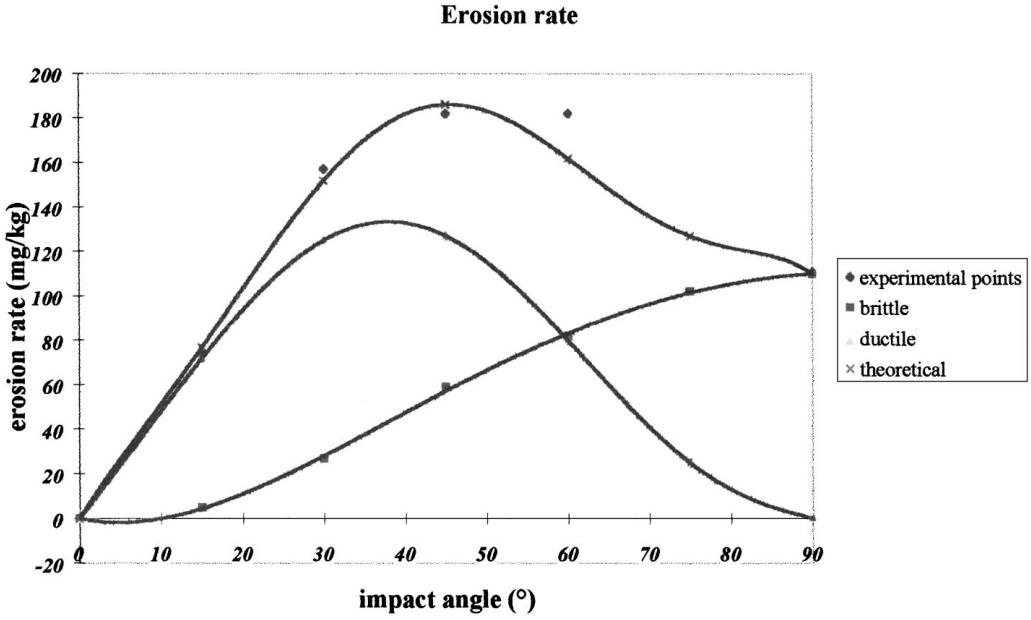

Figure 15 Erosion rate versus impact angle.

conditions a steady-state regime is established, as indicated by the linear variation of the erosion rate versus projected mass (Fig. 16). Hardening results from a twinning phenomenon, as shown by microscopic observations (Fig. 19) and as previously mentioned when other kinds of plastic deformation are performed (see above).

6.3. Discussion

Usually, materials with a high erosion resistance are ductile materials containing a hard phase, for example composites with tungsten carbides or some class of cast irons [27].

In these ferrous alloys, the presence of the hard cementite lamellas improves the wear resistance. This resistance increases with the volume fraction of these lamellas. A similar tendency was reported in WC/Co coatings, when the ratio carbide/matrix was increased up to 90% [24, 25]. However, the most spectacular result was achieved in an austenitic cast iron [27]: impact of particles induced a martensitic transformation in the surface layer (this transformation increases the resistance to digging and micro-machining), while the underlying layer remained austenitic (and hence ductile, therefore accommodating stresses induced by shocks on the surface. Formation of cracks was delayed.

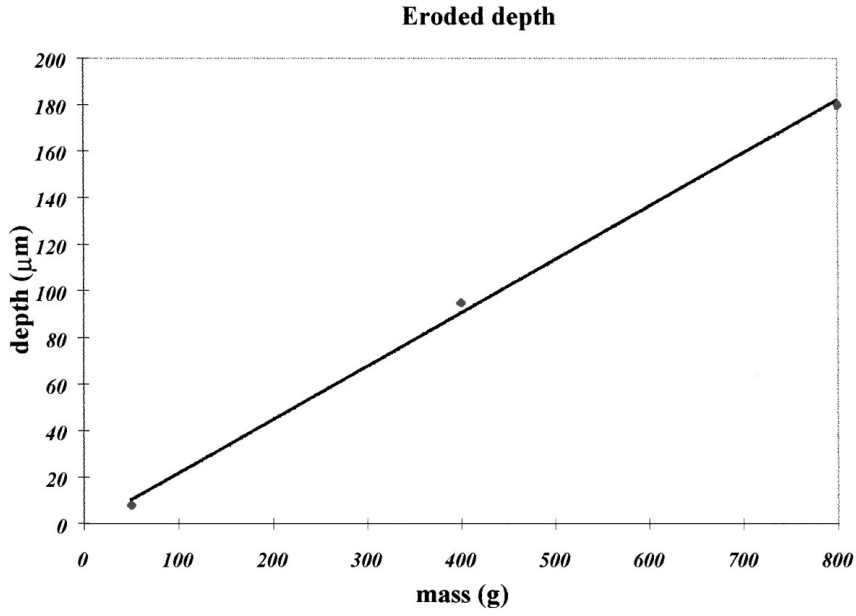

Figure 16 Depth of the eroded zone versus projected mass.

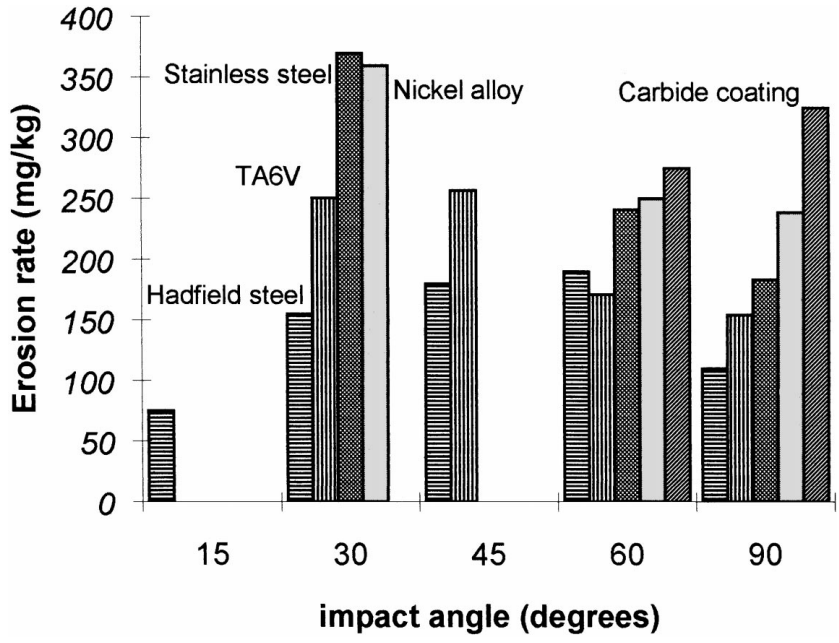

Figure 17 Erosion rate of various materials.

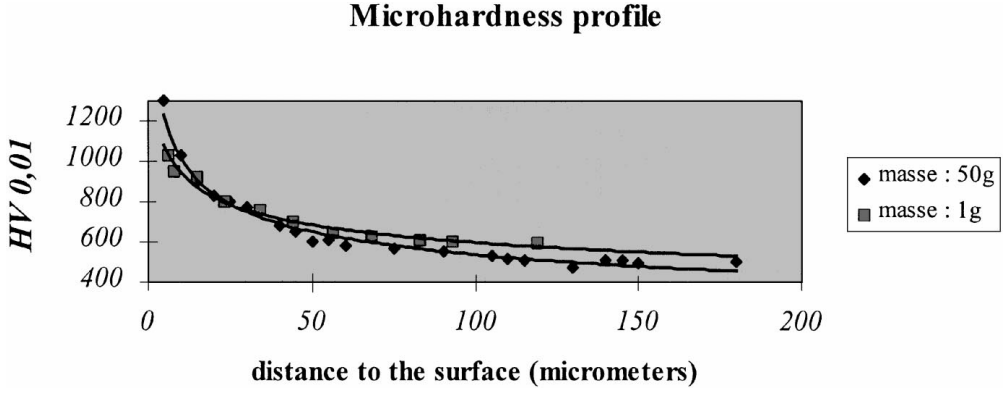

Figure 18 Hardness profile after an erosion test (projected mass: 1 g and 50 g).

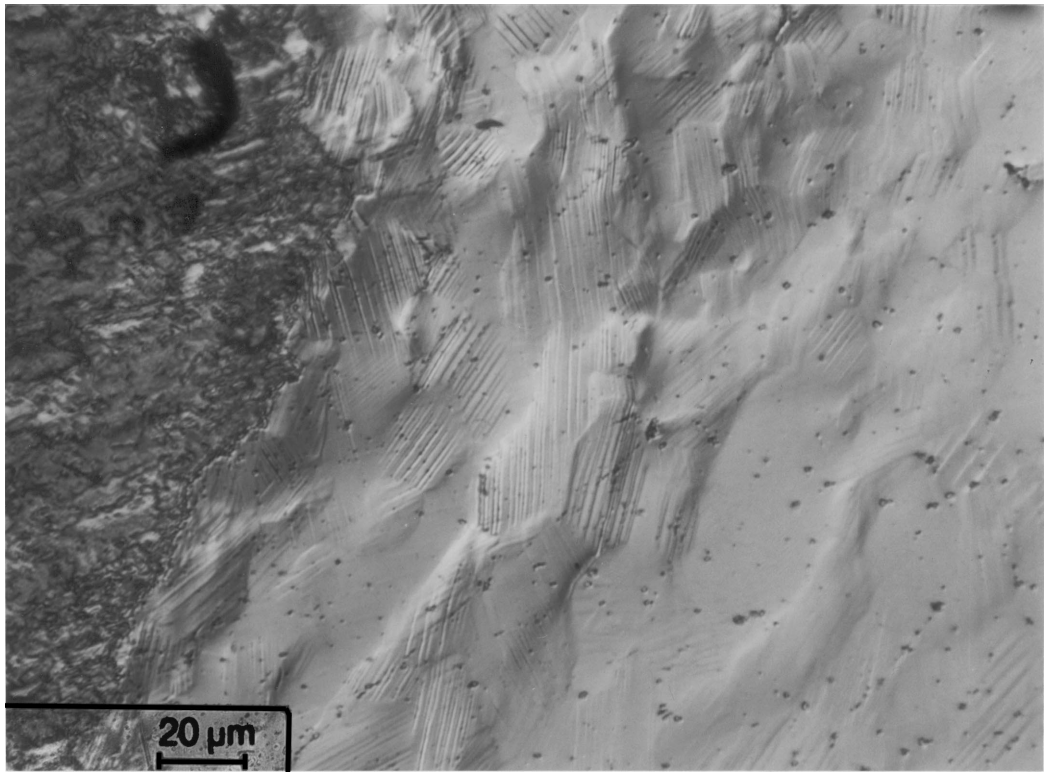

Figure 19 Twin after an erosion test.

Hadfield steel coatings have also an austenitic structure (face centred cubic); in this case the mechanism of the good erosion resistance is not a martensitic transformation, but more probably a twining phenomenon (see above). The most attractive result is that this multilayer structure (brittle layer: ductile layer) is created and maintained as long as the erosion mechanism is progressing.

6.4. Conclusion

Hadfield steel appears like a model material regarding the erosion resistance. Indeed, during impact of eroding particles, the brittle surface layer is always sustained by the underlying ductile layer, yielding therefore to an optimum erosion resistance. Compared to classical multilayer constituted by an alternative stacking of brittle and ductile layers, the ordering of which is progressively destroyed during the erosion test, Hadfield steel behaves like a smart and adaptative material.

7. Conclusion

In this study, it has been shown that when suitable powder is fed continuously into the CO_2 laser beam and propelled at high velocity onto a prepared workpiece, manganese-rich steel cladding (Hadfield steel cladding) can be manufactured with the following features:

—sound layers are achieved, with a thickness up to 1 mm in a single pass.

—a dendritic microstructure is formed; the crystalline structure is austenitic, with a lattice parameter close to that of an austenitic stainless steel.

—the hardness directly after manufacturing is about 350 HV.

—a rapid work-hardening phenomenon occurs during plastic deformation. After cold rolling up to 80%, a large hardness increase is observed (up to 800 HV), without deleterious cracking.

—the behaviour during fretting tests is satisfactory: loading can correspond either to the elastic or to the plastic range, in any case fretting wear is limited and delayed. This good behaviour could result from the work-hardening phenomenon itself, which probably induces a twinning phenomenon.

—the weight loss during an erosion test is low and nearly independent of particle impact angle, corresponding, therefore, to an intermediate behaviour between a ductile and a brittle behaviour. During the impact of eroding particles, cladding present a hard surface with a ductile underlying layer, giving rise to an optimum erosion resistance.

In conclusion, claddings offering ample opportunities for applications where wear resistance is of major importance.

Acknowledgements

The authors would like to thank P. Sallamand and S. Asika for experimental assistance.

References

1. W. M. STEEN, "Laser Material Processing" (Springer Verlag, Berlin, 1991), pp. 172–219.
2. J. M. PELLETIER, P. SALLAMAND and B. CRIQUI, *Lasers in Engineering* **3** (1994) 15.
3. B. E. KIVINEVA, D. L. OLSON and D. K. MAZTLOCK, *Welding Research Suppl.* **3** (1995) 83.
4. J. M. YELLUP, *Surface and Coating Technology* **741** (1995) 121.
5. P. SALLAMAND and J. M. PELLETIER, *Mater. Sci. Eng.* **A171** (1993) 263.

6. J. SINGH and J. MAZUMDER, *Acta Metall.* **35** (1987) 1995.
7. K. NAGARATHNAM and K. KOMVOPOULOS, *Metall. Trans.* **26A** (1995) 2131.
8. Y. N. LIANG, Z. Y. MA, S. Z. LI, S. LI and J. BI, *J. Mater. Sci. Lett.* **14** (1995) 114.
9. F. BONOLLO, L. GIORDANO, I. TANGRINI, A. TIZIANI, N. L. YANG and A. ZAMBON, *La Metallurgia Italiana* **85** (1993) 85.
10. A. T. ALPAS and J. ZHANG, *Metall. Trans.* **25A** (1994) 969.
11. R. J. ARSENAULT and N. SHI, *Mater. Sci. Eng.* **96** (1986) 77.
12. R. BULLOUGH and L. D. DAVIS, *Acta Metall. Mater.* **43** (1995) 2737.
13. J. LLORCA, *ibid.* **42** (1994) 151.
14. E. BAYRAKTAR, C. LEVAILLANT and S. ALTINTER, *J. Phys. III* **C7** (1993) 61.
15. *Idem., J. Mater. Proc. Technol.* **47** (1994) 13.
16. J. M. PELLETIER, M. C. SAHOUR, M. PILLOZ and A. B. VANNES, *J. Mater. Sci.* **28** (1993) 5184.
17. J. M. PELLETIER, A. ISSA and F. FOUQUET, *J. Phys. III* **C7** (1991) 87.
18. P. SALLAMAND and J. M. PELLETIER, *ibid.* **C4** (1994) 155.
19. V. MALAU, Thesis, Ecole Centrale de Lyon, 1996.
20. P. BLANCHARD, C. COLOMBIÉ, V. PERRIN, S. FAYEULLE and L. VINCENT, *Metall. Trans.* **4** (1991) 157.
21. Z. R. ZHOU, S. FAYEULLE and L. VINCENT, *Wear* **155** (1992) 317.
22. C. COLOMBIÉ, Thesis, Ecole Centrale de Lyon, France, 1986.
23. S. FOUVRY, Thesis, Ecole Centrale de Lyon, France, 1997.
24. P. CHEVALLIER, Thesis, Ecole Centrale de Lyon, France, 1994.
25. P. CHEVALLIER, Y. GACHON and A. B. VANNES, Colloque du CEM, Saint-Etienne, November 1994.
26. J. H. NEILSON and A. GILCHRIST, *Wear* **11** (1968) 111.
27. K. SHIMIZU and T. NOGUCHI, *ibid.* **176** (1994) 255.
28. M. GODET, Y. BERTHIER, J. M. LEROY, L. FLAMAND and L. VINCENT, "Mechanical Aspects of Coatings," edited by D. Dowson *et al*. (Elsevier Tribology Series, 1990).

Received 6 October 1997
and accepted 8 October 1998